RSC Advances

PAPER

View Article Online
View Journal | View Issue



Cite this: *RSC Adv.*, 2019, **9**, 5692

# Comparative research on three types of MIL-101(Cr)-$SO_3H$ for esterification of cyclohexene with formic acid

Lijuan Ma,[a] Luo Xu,[a] Haoran Jiang[a] and Xia Yuan *[ab]

Received 18th December 2018
Accepted 5th February 2019

DOI: 10.1039/c8ra10366f

rsc.li/rsc-advances

MIL-101(Cr)-$SO_3H$ was prepared by a one-pot synthesis method using $CrO_3$ or $Cr(NO_3)_3 \cdot 9H_2O$ as a Cr source and 2-sulfoterephthalic acid monosodium salt as a ligand with three different mineralizers, HCl, HF and NaAC, respectively. Among the prepared catalysts, MIL-101(Cr)-$SO_3H$, which uses HCl as a mineralizer, has a high specific surface area and the strongest acidity compared with the other two mineralizers. When these catalysts were used to catalyze the esterification of cyclohexene with formic acid, MIL-101(Cr)-$SO_3H$ prepared using HCl as a mineralizer possessed the highest catalytic activity in the esterification, because the conversion rate of cyclohexene is 63.97%, whereas MIL-101(Cr)-$SO_3H$ prepared using NaAC and HF as a mineralizer shows cyclohexene conversion rates of 38.40% and 32.46%, while their selectivity to cyclohexyl formate is about 97.50%. MIL-101(Cr)-$SO_3H$ with HCl as a mineralizer can be reused three times in succession without any loss of catalytic activity.



## 1. Introduction

Cyclohexanol is used widely to produce adipic acid, caprolactam, hexamethylene diamine and cyclohexanone.[1] The main processes for the production of cyclohexanol are based on the oxidation of cyclohexane,[2,3] the hydrogenation of phenol,[1] and the direct hydration of cyclohexene.[4] The cyclohexane oxidation process is used mainly in industry, but it is hazardous. And phenol hydrogenation, as the oldest method of cyclohexanol production, is subject to greater restrictions in industrial application due to the high cost of raw materials and the consumption of large amounts of hydrogen and energy. In addition, although direct hydration is highly selective, increasing economic benefits to a certain extent and reducing the possibility of danger in the two traditional production processes, it allows only a very low conversion per pass, because of slightly exothermic and equilibrium limited.[5]

To overcome the main problem of the thermodynamic equilibrium limitation of the direct hydration reaction of cyclohexene, the indirect hydration of cyclohexene was born out, which is a two-step process using formic acid as a reactive entrainer.[6–9] In the first step, cyclohexene react with formic acid to produce cyclohexylformate, which is an electrophilic addition esterification,[10] needing acid catalyst to increase the conversion rate of cyclohexene. In the second step, the ester readily hydrolyzes to produce cyclohexanol. Steyer *et al.*[5,6,11] simulates the indirect hydration process using two distillation towers. Sulfonic-acid resin Amberlyst-15 catalyzed the esterification of cyclohexene with formic acid in the first distillation tower, the hydrolysis of cyclohexyl formate occurred in the second column. Cyclohexene conversion reached about 100%. But distillation tower costs highly, and sulfonic-acid resin Amberlyst-15 deactivates and swells easily. Imam *et al.*[7] evaluated indirect hydration process, agreed that the energy consumption of the process is much lower than direct hydration process. Du *et al.*[12] used HZSM-5 as catalysts in indirect hydration, and obtained cyclohexanol yields of up to 40%, which was far more than in the direct hydration of cyclohexene, and HZSM-5 could be reused without apparent inactive. Previous studies have shown that the hydrolysis reaction of ester occurs easily, the addition esterification of cyclohexene with formic acid by acid catalyst is the key step to realize the indirect hydration.[5]

Sulfonic acid is a very strong organic acid, which acidity is similar to that of general inorganic acids. Sulfonic-acid resin Amberlyst-15 (ref. 13) worked well, but it swelled and could not be reused. The introduction of sulfonic groups into inorganic carriers has attracted the attention of researchers. There are a number of sulfonic acid functionalized catalysts are used in acid-catalyzed reactions, and performed successfully great catalytic activity and recyclability, including cellulose hydrolysis reaction,[14] heterogeneous alcoholysis reaction,[15] acetal reaction,[16] partial esterification reaction.[17,18] Among them, SBA-15-$SO_3H$[19,20] can be reused to some extent in some acid-catalyzed reactions, but the grafted sulfonic-acid group is limited because of the limited content of Si–OH on the carrier of the SBA-15 molecular sieve. Furthermore, the distribution of

[a]*College of Chemical Engineering, Xiangtan University, Xiangtan 411105, Hunan, China. E-mail: yxiamail@163.com; Tel: +86-731-58293545*

[b]*National & Local United Engineering Research Centre for Chemical Process Simulation and Intensification, Xiangtan 411105, China*

sulfonic-acid groups is not uniform, which results in the reaction solution not being in sufficient contact with the active component during the reaction.

Metal–organic frameworks (MOFs),[17,18,21,22] as porous crystalline materials, have high specific surface area, large pore volume, and the advantages of more regular structure and easy modification by functional organic ligands. Since Férey prepared successfully MIL-101(Cr) using HF as mineralizer that can not only increase the solubility of terephthalic acid in solvent but also regulate the nucleation rate of catalysts,[23] many researchers began to notice its prominence. MIL-101(Cr) has higher specific surface area and larger pore volume than other MOFs, and it overcomes the disadvantages of poor thermal and chemical stability of other MOFs,[23–25] which make it a focus. Huang *et al.*[26] synthesized MIL-101(Cr) by NaAC as mineralizer, and discovered that it had better thermostability than prepared by HF as mineralizer.

According to that MIL-101(Cr)[23,26] can be prepared by different mineralizers and resulted in different performance, we synthesized MIL-101(Cr)-$SO_3H$ by HF, NaAC as mineralizer, respectively. In addition, George Akiyama prepared MIL-101(Cr)-$SO_3H$ using HCl as mineralizer, which showed high durability to boiling water and distinct and clean catalytic activity for the cellulose hydrolysis reaction, with a strong Brønsted acid site on its pore surface.[14] And we also used HCl to synthesize MIL-101(Cr)-$SO_3H$. We just researched *in situ* synthesis method, because the catalytic activity of MIL-101(Cr)-$SO_3H$ prepared by the post-modification method is inferior to the one-step synthesis of MIL-101(Cr)-$SO_3H$.[18] In addition, these three types of MIL-101(Cr)-$SO_3H$ were catalyzed the esterification of cyclohexene with formic acid for the first time.

## 2. Experimental section

### 2.1 Materials and chemicals

All solvents and reactants were from commercially available sources and were used without further purification. Chromium nitrate nonahydrate, chromium oxide, terephthalic acid, fomic acid and cyclohexene (AR, 98%) were from Macklin (China). Hydrofluoric acid (AR, 40%), 37% fuming hydrochloric acid, sodium acetate, concentrated sulfuric acid (AR, 98%), ethanol and acetone were from Sinopharm Chemical Reagent Co., Ltd (China). Monosodium 2-sulfoterephthalic acid was from TCI (Shanghai) Development Co., Ltd., respectively.

### 2.2 Catalyst preparation

**2.2.1 MIL-101-$SO_3H_{HCl}$ synthesis.** According to the procedure by Akiyama and co-workers,[14] a mixture of monosodium 2-sulfoterephthalic acid (2 g, 7.5 mmol), $CrO_3$ (0.75 g, 7.5 mmol) and concentrated aqueous hydrochloric acid (12 N, 0.546 g) were dissolved in water (30 g), and the mixed solution was treated hydrothermally at 453 K for 6 d. The cooling prepared solid solution was washed three times each with ethanol and deionized water and after centrifugal separation and vacuum drying for 6 h at 150 °C, the obtained green powder was denoted MIL-101-$SO_3H_{HCl}$.

**2.2.2 MIL-101-$SO_3H_{HF}$ synthesis.** A mixture of chromium(III) nitrate nonahydrate (2.00 g, 5 mmol), monosodium 2-sulfoterephthalic acid (2.70 g, 10 mmol), deionized water (30 g) and hydrofluoric acid (47–51 wt%, 0.3 g) were heated for 24 h at 463 K. The cooling prepared solid solution was washed three times each with ethanol and deionized water and a green powder was obtained by centrifugal separation and vacuum drying for 6 h at 150 °C. The synthesized green powder was termed MIL-101-$SO_3H_{HF}$.[27] When we replaced monosodium 2-sulfoterephthalic acid with terephthalic acid, the resulting green powder was denoted MIL-101(Cr).

**2.2.3 MIL-101-$SO_3H_{NaAC}$ synthesis.** A mixture of chromium(III) nitrate nonahydrate (2.00 g, 5 mmol), monosodium 2-sulfoterephthalic acid (2.70 g, 10 mmol), deionized water (30 g) and sodium acetate (0.12 g, 0.9 mmol) were heated at 463 K for 24 h. The cooling prepared solid solution was washed three times each with ethanol and deionized water and a green powder was obtained by centrifugal separation and vacuum drying for 6 h at 150 °C. The synthesized green powder was termed MIL-101-$SO_3H(Na)_{NaAC}$.

MIL-101(Cr)-$SO_3H(Na)_{NaAC}$ (1 g) was added to 5 g 0.1 mol $L^{-1}$ $H_2SO_4$ solution and 10 mL ethanol, stirred at room temperature for 24 h, and washed with ethanol until the washing solution became neutral. Finally, the green powder was dried in vacuum for 6 h at 150 °C.[28] The resulting sulfonic acid-functionalized MIL-101 was termed MIL-101-$SO_3H_{NaAC}$.

### 2.3 Characterization

Powder X-ray diffraction (XRD) patterns were obtained on a D/Max-2500 diffractometer using Cu-Kα radiation from 2–14° with a step size of 0.02°. The textural properties of the prepared samples were outgassed for 4 h at 423 K and determined by $N_2$ adsorption at 77 K, using a NOVA 2200e instrument (Quanta chrome, USA). The infrared (IR) spectra were collected on a Thermo Nicolet 380 Fourier transform infrared (FT-IR) spectrophotometer in KBr disks at room temperature. Thermal stability analysis was performed from 30 °C to 800 °C at 10 °C $min^{-1}$, using a TGA/DSC/1600HT analyzer (Mettler Toledo, Switzerland). The S content in the catalysts was measured by using an Elementar Vario EL III analyzer; and the Na and Cr contents were measured by Thermo Jarrell Asch IRIS Advantage 1000 inductively coupled plasma-atomic spectroscopy. The acid strength and the amount of acid on the catalysts was determined by ammonia-temperature-programmed desorption ($NH_3$-TPD), in which samples were programmed from 80 °C to 700 °C at 10°C $min^{-1}$. X-ray photoelectron spectroscopy (XPS) spectra were acquired with a Kratos Axis UltraDLD spectrometer (Kratos Analytical-A, Shimadzu group company) using a monochromatic Al K150 W X-ray source. The analysis chamber pressure was less than $5 \times 10^{-9}$ torr. An energy step size of 0.1 eV was chosen for the survey spectra. The BE scale was calibrated according to the C 1s peak (284.8 eV) of adventitious carbon on the analyzed sample surface. Peak fitting was carried out on the basis of Gaussian functions.

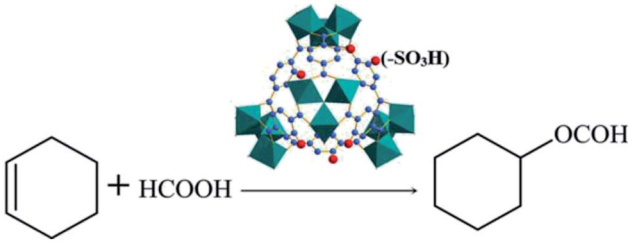


Scheme 1 Equation of the esterification of cyclohexene with formic acid over MIL-101(Cr)-$SO_3H$.

### 2.4 Esterification of cyclohexene with formic acid

Cyclohexene (4.11 g) and formic acid (6.90 g) were added sequentially to a three-necked round-bottom flask in a 1 : 3 molar ratio, and the amount of catalyst (0.55 g) used was 5% of the total mass of the reactants. The reaction mixture was stirred magnetically at 80 °C in an oil bath for 6 h. After the reaction, the solution was cooled to room temperature, an appropriate amount of acetone solvent was added to the three-necked flask, and the reaction liquid was mixed to a single phase by stirring for 30 min.[19] The supernatant liquid sample was used to determine the conversion rate of cyclohexene and the selectivity of cyclohexyl formate by gas chromatography using an Agilent 7890 instrument with a HP-5 capillary column and FID indicator. The used catalyst was dried in vacuum at 423 K for 12 h, before being used in consecutive runs. The equation for the reaction of cyclohexene with formic acid is as shown in Scheme 1.

## 3. Results and discussion

### 3.1 Characterization of fresh catalyst samples

**3.1.1 Nitrogen adsorption.** $N_2$ adsorption isotherms measured at 77 K (Fig. 1A) reveal two characteristic steps of the MIL-101-$SO_3H$ that are related to the filling of the mesoporous and microporous cavities. The adsorption of MIL-101-$SO_3H_{NaAC}$ increased most rapidly at all pressure stages, which indicates that MIL-101-$SO_3H_{NaAC}$ contains more mesopores than the other two. And the pore-size-distribution curve of the different samples confirms the above discussion (Fig. 1B).[16,29] The specific surface area and pore-diameter distribution of the samples is shown in Table 1. Based on a comparison of the parameters, the specific surface area of the MIL-101-$SO_3H_{HF}$ is maximum, the specific surface area of MIL-101-$SO_3H_{NaAC}$ and MIL-101-$SO_3H_{HCl}$ are similar and a little smaller than MIL-101-$SO_3H_{HF}$, while their pore volume characteristics show that MIL-101-$SO_3H_{HF}$ has most micropores and MIL-101-$SO_3H_{NaAC}$ contains most mesopores.

**3.1.2 FT-IR characterization.** The FT-IR results of the different samples in Fig. 2 show that MIL-101-$SO_3H$ and MIL-101(Cr) are essentially identical in their infrared characteristic peak positions. The characteristic peak of MIL-101(Cr)-$SO_3H$ at 1182 $cm^{-1}$ belongs to the antisymmetric vibration of O=S=O, whereas the symmetric stretching vibration occurs at 1228 $cm^{-1}$. The benzene ring skeleton vibration in-plane of the sulfonic acid substitution occurs at 1084 $cm^{-1}$, whereas 1024 $cm^{-1}$ is the strong stretching vibration of S–O and 623 $cm^{-1}$ is the stretching vibration peak of C–S.[30,31] It can be concluded that the sulfonic acid groups were grafted successfully onto the MIL-101(Cr), regardless of which of the three mineralizers was used.

**3.1.3 Elemental analysis.** Table 2 shows that MIL-101-$SO_3H_{HCl}$ has the highest content of S and Cr and the least $Na^+$, whereas MIL-101-$SO_3H(Na)_{NaAC}$ has the largest amount of $Na^+$ because of the introduction of $Na^+$ in the mineralizer and although the acidified MIL-101-$SO_3H_{NaAc}$ possessed slightly less $Na^+$, it was still higher than the other two samples. It is worth noting that the S content was also reduced after acidification, which results because the elemental S cannot be retained perfectly because much of the $Na^+$ had fallen off. This result indicates that MIL-101-$SO_3H_{HCl}$ has the maximum number of active groups.

**3.1.4 XRD analysis.** The obtained samples exhibited strong diffraction peaks (Fig. 3) at $2\theta$ = 2.77°, 3.30°, 5.10°, 8.40°and 9.00°, which corresponds to the crystal-plane diffraction of 311, 511, 531, 882 and 911, which are typical diffraction peaks for

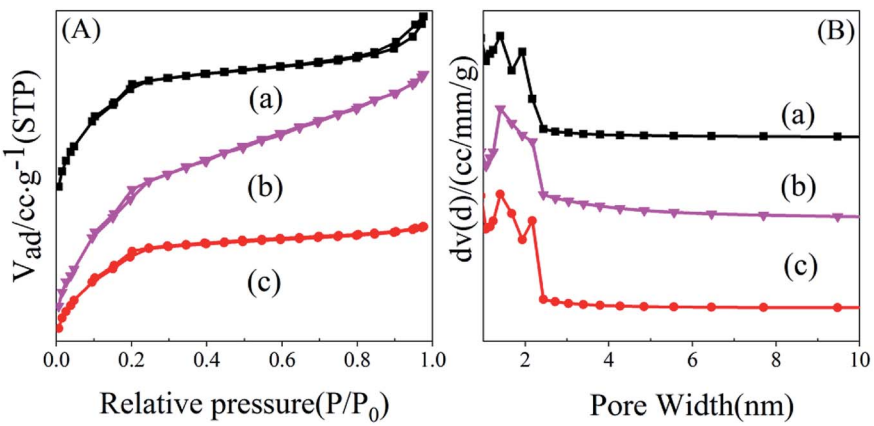


Fig. 1 Nitrogen adsorption isotherms (A) and pore diameter distribution (B) of samples. (a) MIL-101-$SO_3H_{HCl}$, (b) MIL-101-$SO_3H(Na)_{NaAC}$, (c) MIL-101-$SO_3H_{HF}$.

Table 1 Nitrogen physical adsorption data of samples

| Sample | $S_{BET}$ ($m^2\ g^{-1}$) | $V_P$ mesoporous ($cm^3\ g^{-1}$) | $V_P$ micropore ($cm^3\ g^{-1}$) |
|---|---|---|---|
| MIL-101-$SO_3H_{HCl}$ | 1362 | 1.117 | 0.573 |
| MIL-101-$SO_3H_{NaAc}$ | 1376 | 1.547 | 0.381 |
| MIL-101-$SO_3H_{HF}$ | 1501 | 1.159 | 0.631 |

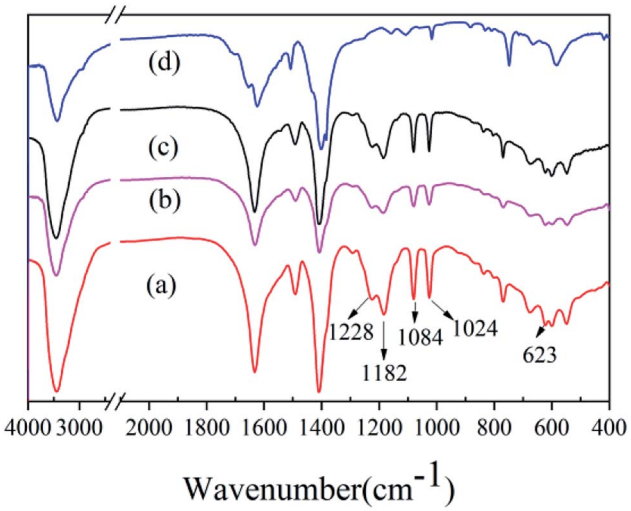


Fig. 2 FT-IR spectra of various catalysts. (a) MIL-101-$SO_3H_{HCl}$, (b) MIL-101-$SO_3H(Na)_{NaAC}$, (c) MIL-101-$SO_3H_{HF}$, (d) MIL-101.

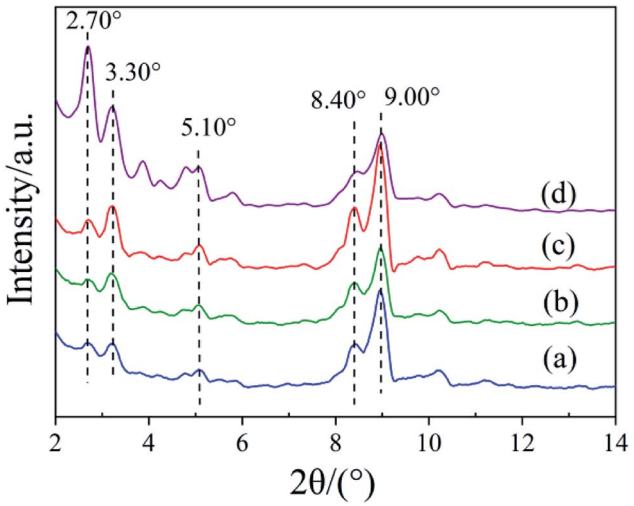


Fig. 3 XRD patterns of various catalysts. (a) MIL-101-$SO_3H_{HCl}$, (b) MIL-101-$SO_3H(Na)_{NaAC}$, (c) MIL-101-$SO_3H_{HF}$, (d) MIL-101-$SO_3H_{NaAC}$.

MIL-101 (Cr).[23] This result indicates that the prepared MIL-101(Cr)-$SO_3H$ has the same crystal-phase structure as the MIL-101(Cr), which correlates with the FT-IR characterizations. By comparison, the MIL-101(Cr)-$SO_3H(Na)_{NaAC}$ and MIL-101(Cr)-$SO_3H_{NaAC}$ samples have a similar crystal structure, but the MIL-101(Cr)-$SO_3H_{NaAC}$ has a stronger diffraction peak at 2–6°. This results because $Na^+$ is replaced by $H^+$ through proton exchange,[15] which yields neater crystal planes, after the acidification process.

**3.1.5 Thermogravimetric analysis.** The significant mass-loss stages of the three samples are shown in Fig. 4. The first mass-loss stage of the three samples at 30–125 °C, belongs mainly to the removal of water temperature from the samples. It is worth noting that the percent weightlessness of MIL-101-$SO_3H_{HCl}$ is the least, that of MIL-101-$SO_3H_{NaAC}$ is a little more and MIL-101-$SO_3H_{HF}$ has the maximum percentage of weightlessness. Thus, MIL-101-$SO_3H_{HCl}$ contains a minimum amount of adsorbed water. Then MIL-101-$SO_3H_{HF}$ has a clear second-loss stage at 320–480 °C, because of the proportion of thermal decomposition of the –$SO_3H$ group is much higher than that of the other two,[27] whereas MIL-101-$SO_3H_{HCl}$ and MIL-101-$SO_3H_{NaAC}$ show a low mass loss. The third distinct mass-loss stage of MIL-101-$SO_3H_{HCl}$ and MIL-101-$SO_3H_{NaAC}$ occurred at 410–560 °C, and that of MIL-101-$SO_3H_{HF}$ occurred at 480–660 °C, because the skeleton collapsed after the –$SO_3H$ group decomposed slowly to generate hydride.[32] Comparison of the weight loss of three samples, mass weightlessness of MIL-101-$SO_3H_{HF}$ occurred first, after the removal of water, which indicates the thermal stability of MIL-101-$SO_3H_{HF}$ is worst. And MIL-101-$SO_3H_{HCl}$ has the best stability than the other two.

Table 2 The result of elemental analysis of chromium, sodium and S from the different samples

| Sample | S (wt%) | Cr (wt%) | Na (wt%) | $Na^+/S^{3-}$ |
|---|---|---|---|---|
| MIL-101-$SO_3H_{HCl}$ | 6.79 | 15.72 | 0.73 | 0.11 |
| MIL-101-$SO_3H(Na)_{NaAC}$ | 7.10 | 13.88 | 2.65 | 0.37 |
| MIL-101-$SO_3H_{NaAc}$ | 6.05 | 13.8 | 2.04 | 0.34 |
| MIL-101-$SO_3H_{HF}$ | 5.93 | 12.73 | 1.96 | 0.33 |

**3.1.6 $NH_3$-TPD analysis.** To demonstrate the difference in acidity of the three samples, $NH_3$-TPD was used for characterization analysis (Fig. 5). To eliminate the signal effects that are caused by the high-temperature decomposition of samples, MIL-101-$SO_3H(Na)_{NaAC}$ was processed in the temperature program without $NH_3$ adsorption. The peak plot of MIL-101-$SO_3H(Na)_{NaAC}$ (does not adsorb $NH_3$) was divided into three peaks termed '1', '2', '3' (the peak area ratio is 1.0 : 2.0 : 2.6); these indicate the gradual decomposition performance of the catalyst, and proved the results of the thermogravimetric analysis. The $NH_3$-TPD peak diagram of MIL-101-$SO_3H(Na)_{NaAC}$ was divided into five peaks (the peak area ratio is 0.3 : 1.0 : 1.5 : 2.0 : 2.6), the peak labeled '4' represents a weak acidity, and the peak labeled '5' manifests a medium–strong acidity. The five peaks of MIL-101-$SO_3H_{NaAC}$ (the peak area ratio is 0.2 : 1.0 : 2.2 : 2.0 : 2.6) show that its medium–strong acidity

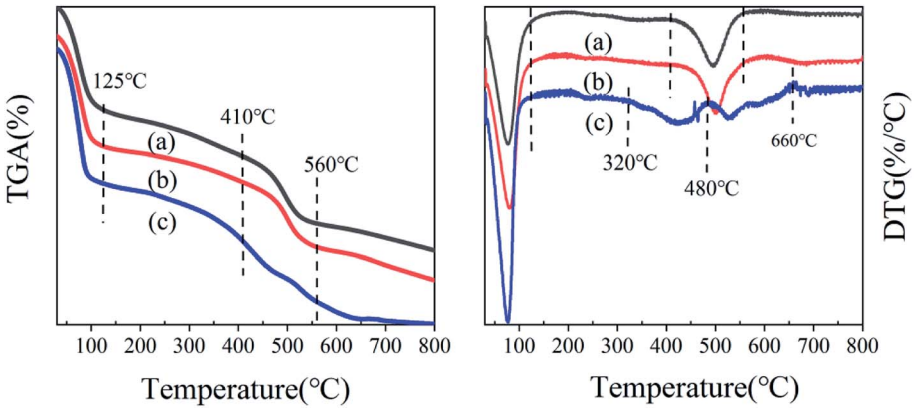


Fig. 4 Thermogravimetric thermogram of various catalysts. (a) MIL-101-$SO_3H_{HCl}$, (b) MIL-101-$SO_3H(Na)_{NaAC}$, (c) MIL-101-$SO_3H_{HF}$.

is stronger than that of MIL-101-$SO_3H(Na)_{NaAC}$, because more active components result from proton exchange of $Na^+$ and $H^+$. A weak and medium–strong acidity exist in the MIL-101-$SO_3H_{HCl}$ (the peak area ratio is 0.3 : 1.0 : 2.2 : 2.0 : 2.6) and MIL-101-$SO_3H_{HF}$ (the peak area ratio is 0.2 : 1.0 : 1.4 : 2.0 : 2.6). For comparison, MIL-101-$SO_3H_{HF}$ has the least amount of medium–strong acidity, and MIL-101-$SO_3H_{HCl}$ has more proportion of weak acidity than MIL-101-$SO_3H_{NaAC}$.Therefore, combined with the previous discussion, MIL-101-$SO_3H_{HCl}$ is strongest in acidity and thermal stability.

**3.1.7 XPS analysis.** The elemental C, O, Cr, S and F in MIL-101-$SO_3H$ are shown in Fig. 6A. A peak appears at 168 eV for S 2p, which indicates that all three samples contain sulfonic-acid groups. The split peak of S 2p with peak positions at 169.0 eV and 167.8 eV belongs to the peaks of R–$SO_3H$ and R–$SO_3R'$, respectively.[33] The ratio of peak distribution on the sample surfaces show that the proportion of MIL-101-$SO_3H(Na)_{NaAC}$ (the peak area ratio is 1 : 1.62) is smallest, MIL-101-$SO_3H_{HCl}$ (the peak area ratio is 1 : 1.58) is slightly smaller, and MIL-101-$SO_3H_{HF}$ (the peak area ratio is 1 : 1.54) is largest. The Cr 2p has two peaks at 587.1 eV and 577.3 eV, respectively, which are typical Cr $2p_{1/2}$, Cr $2p_{3/2}$ split peaks,[34] and the peak distribution ratio of these three catalysts is not much different, whereas the proportion of MIL-101-$SO_3H(Na)_{NaAC}$ (the peak area ratio is 1.8 : 1) is reduced slightly compared with that of MIL-101-$SO_3H_{HCl}$ (the peak area ratio is 1.9 : 1) and MIL-101-$SO_3H_{HF}$

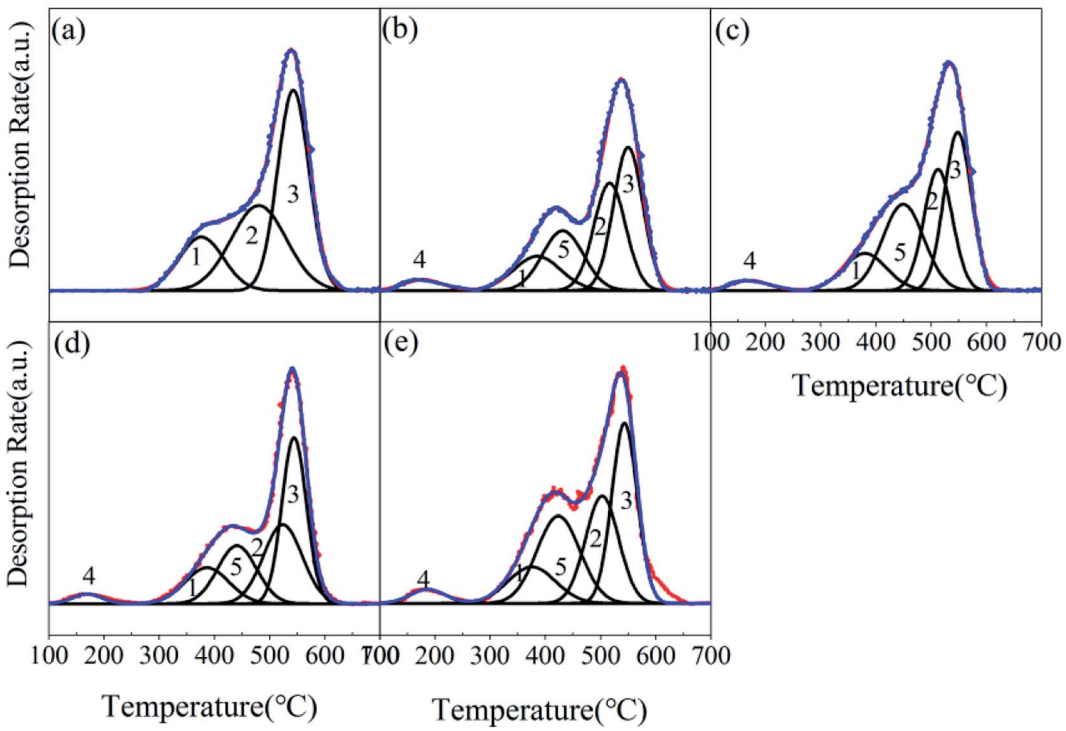


Fig. 5 $NH_3$-TPD peak separation curve of four samples (a) MIL-101-$SO_3H(Na)_{NaAC}$ (don't adsorb $NH_3$), (b) MIL-101-$SO_3H(Na)_{NaAC}$, (c) MIL-101-$SO_3H_{NaAc}$, (d) MIL-101-$SO_3H_{HF}$, (e) MIL-101-$SO_3H_{HCl}$.

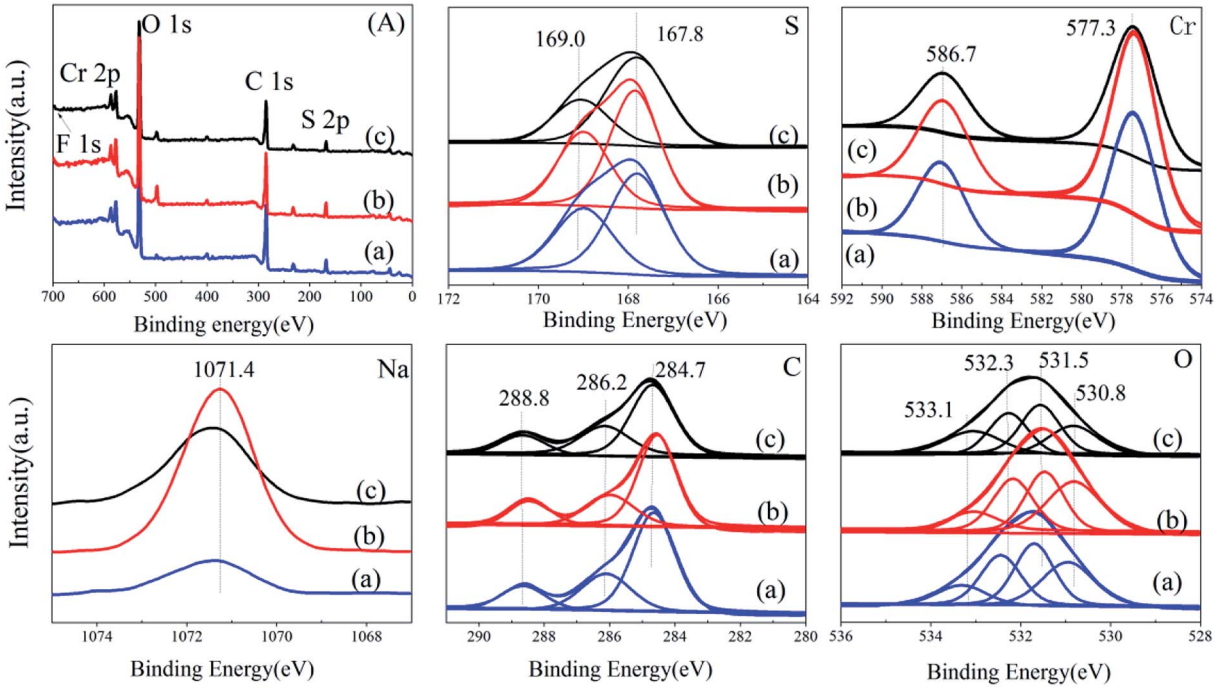


Fig. 6 XPS spectra of various samples (A) survey spectrum. (a) MIL-101-$SO_3H_{HCl}$, (b) MIL-101-$SO_3H(Na)_{NaAC}$, (c) MIL-101-$SO_3H_{HF}$.

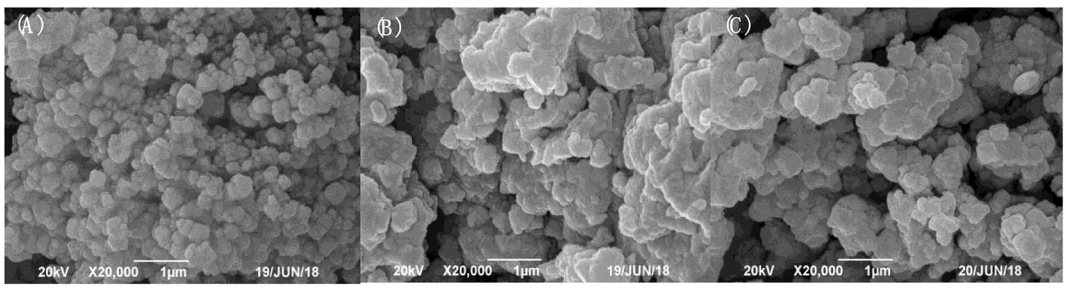


Fig. 7 SEM of three catalysts. (A) MIL-101-$SO_3H_{HCl}$, (B) MIL-101-$SO_3H_{NaAC}$, (C) MIL-101-$SO_3H_{HF}$.

(1.9 : 1). Moreover, the peaks of Na 1s in the three samples clearly prove that MIL-101-$SO_3H(Na)_{NaAC}$ contains the maximum $Na^+$, whereas MIL-101-$SO_3H_{HCl}$ contains minimal $Na^+$. Only MIL-101-$SO_3H_{HF}$ has a small peak of F 1s at 164.2 eV, which indicates that $F^-$ is involved in the construction of the framework in the synthesized catalyst.[35] However, the split

Table 3 Results of catalytic performance evaluation of catalyst[a]

| Sample | Acid density (mmol $g^{-1}$) | Cyclohexene conversion (%) | Cyclohexylformate selective (%) | Literature |
|---|---|---|---|---|
| MIL-101 | — | 5.30 | 67.15 | This work |
| MIL-101-$SO_3H_{HCl}$ | 0.82 | 63.97 | 97.61 | This work |
| MIL-101-$SO_3H_{HF}$ | 0.73 | 38.40 | 97.34 | This work |
| MIL-101-$SO_3H_{NaAc}$ | 0.76 | 32.46 | 97.71 | This work |
| SBA-15-$SO_3H$ | 0.23 | 54.40 | 95.80 | 19 and 20 |
| PSCSA[b] | 0.81[c] | 87.80 | 97.40 | 10 |
| HZMS-5[b] | 1.70 | 77.60 | 97.00 | 12 |
| Nafion NR50[b] | 0.51 | 68.20 | 98.50 | 19 |
| Amberlyst-15 | 4.60 | 91.50 | 98.10 | 18 |

[a] Reaction conditions: cyclohexene = 4.11 g, $n$(cyclohexene) : $n$(HCOOH) = 1 : 3, $m$(catalyst) = 0.55 g, 80 °C, 6 h. Acid densities were calculated by elemental analysis and XPS. [b] Reaction was conducted into the autoclave at 413 K. [c] Based on S content by elemental analysis.

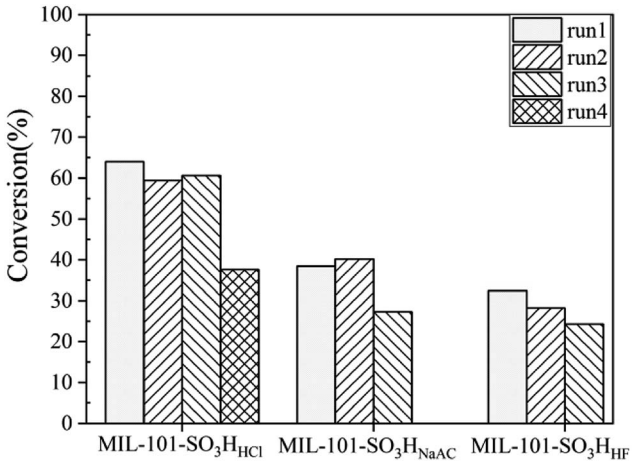


Fig. 8 The reusability of the three catalysts.

peaks of other elements show no clear difference. Therefore, with NaAC as a mineralizer, the introduction of a large amount of $Na^+$ has a significant influence on the surface sulfonic-acid content in MIL-101-$SO_3H$, which results in a decrease in active groups on the catalyst surface.

**3.1.8 SEM morphology.** SEM analysis of the MIL-101-$SO_3H$ prepared by three different mineralizers is shown in Fig. 7. The particle distribution of the three samples is uneven with obvious agglomeration.[36] MIL-101-$SO_3H_{HCl}$ has the smallest particle size, whereas MIL-101-$SO_3H_{HF}$ has the largest particle size, and MIL-101-$SO_3H_{NaAC}$ shows little difference from MIL-101-$SO_3H_{HF}$, which is consistent with the literature.[27]

### 3.2 Catalytic performance

The acidic concentration of the catalyst was calculated by elementary and XPS analysis. The results were listed in Table 3. It is clear that MIL-101-$SO_3H_{HCl}$ has more acid content, and acid activities.

The conversion and selectivity of esterification catalyzed by obtained samples, shows that the MIL-101 exhibited almost no catalytic performance on esterification, and the cyclohexene conversion rate was only 5.30%. The catalytic performance of MIL-101-$SO_3H_{HCl}$ was best, with cyclohexene conversion rate of 63.97%, and cyclohexyl formate selectivity of 97.61%. The catalytic performance of MIL-101-$SO_3H_{NaAC}$ is better than that of MIL-101-$SO_3H_{HF}$. So the $-SO_3H$ is the primary active group in MIL-101-$SO_3H$ and MIL-101-$SO_3H_{HCl}$ performed best in this esterification. And after acidification of the MIL-101-$SO_3$-$H(Na)_{NaAC}$, its catalyst reactivity increases to a certain extent.

Fig. 8 indicates the reusability of the three catalysts evaluated in this work. We can see that MIL-101-$SO_3H_{HCl}$ can be recycled three times and the conversion rate of the esterification reaction remained at 37.6% with the selectivity of cyclohexyl formate keeping almost constant after the third run, whereas the fresh MIL-101-$SO_3H_{NaAC}$ can be only used for two runs and MIL-101-$SO_3H_{HF}$ can keep run once only. The best performance of MIL-101-$SO_3H_{HCl}$ is because of its maximum effective acid content and strongest tolerance compared with the other two, which are both key to determine the catalytic performance in this acid-catalyzed esterification. The poorest stability of MIL-101-$SO_3H_{HF}$ caused its worst productivity. Its fresh sample had started to collapse in the first time of esterification, so even though it has enough acid content, it did not generate the similar great result as MIL-101-$SO_3H_{HCl}$. And the performance of MIL-101-$SO_3H_{NaAC}$ occurred for the same reason. These results also correspond to previous thermogravimetric characterization analysis.

To establish the reason for the instability of MIL-101-$SO_3H$, the sample reusability was analyzed by fundamental characterization. The amount of adsorption of the three samples in the lower-pressure zone was reduced in the $N_2$ adsorption isotherms (Fig. 9A), which indicates that fewer catalyst micropores exist, mainly because the catalytic skeleton collapsed. This result is also suggested by the obvious displacement of the pore-size distribution of the three samples. The specific surface

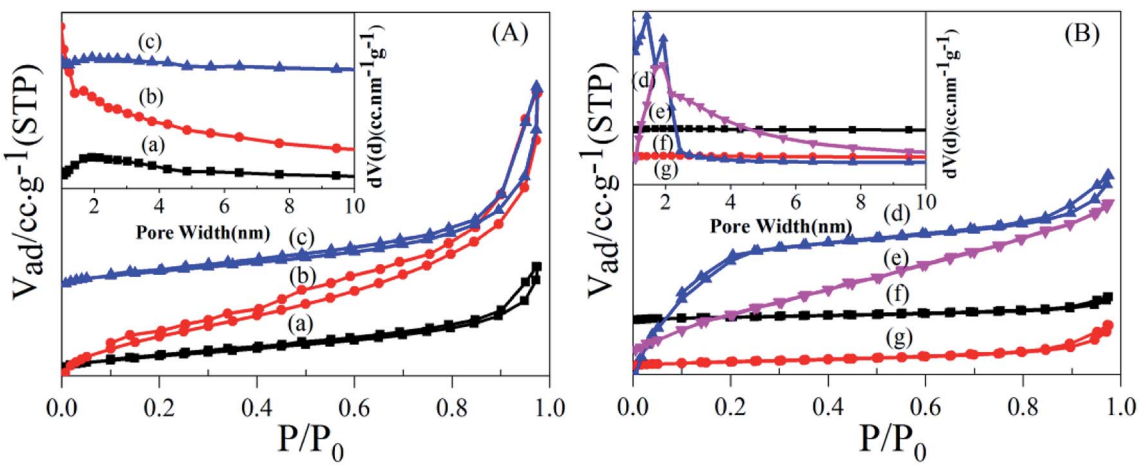


Fig. 9 The $N_2$ isotherms and pore diameter distribution of three catalysts for three run times (A) (a) MIL-101-$SO_3H_{HCl}$, (b) MIL-101-$SO_3H_{NaAC}$, (c) MIL-101-$SO_3H_{HF}$ and MIL-101-$SO_3H_{HCl}$ with different run times (B), (d) fresh MIL-101-$SO_3H_{HCl}$, (e) MIL-101-$SO_3H_{HCl}$ run 1, (f) MIL-101-$SO_3H_{HCl}$ run 3, (g) MIL-101-$SO_3H_{HCl}$ run 5.

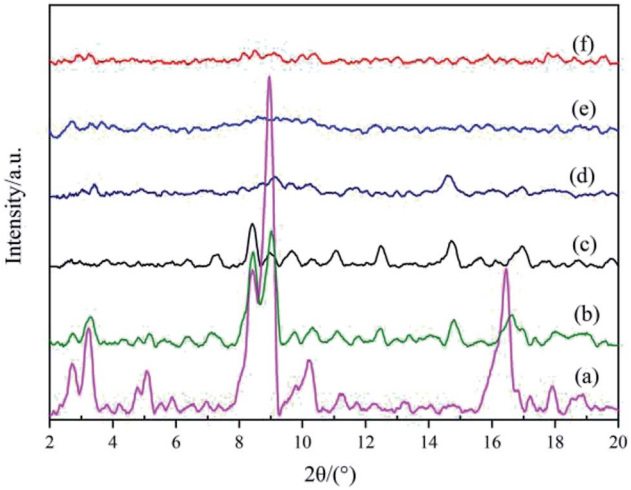


Fig. 10 XRD patterns of three catalysts for recovery in three run times and MIL-101-$SO_3H_{HCl}$ with different run times (a) MIL-101-$SO_3H_{HCl}$ fresh, (b) MIL-101-$SO_3H_{HCl}$ run 1, (c) MIL-101-$SO_3H_{HCl}$ run 3, (d) MIL-101-$SO_3H_{HCl}$ run 5, (e) MIL-101-$SO_3H_{NaAC}$, (f) MIL-101-$SO_3H_{HF}$.

area of the MIL-101-$SO_3H_{HCl}$ (877 $m^2$ $g^{-1}$) was retained after the first run time, but with an increase in run time, the catalyst structure began to change significantly until after the third run. The specific surface area of the fifth recovered catalyst is similarly small to that of the third run at 256 $m^2$ $g^{-1}$ and 124 $m^2$ $g^{-1}$, respectively (Fig. 9B), and the apparent change in pore-size distribution reveals that the catalyst collapsed until there were almost no micropores at the end. XRD patterns of the different MIL-101-$SO_3H$ samples (Fig. 10) show that the crystallinity of the three catalysts after three runs is low. Although MIL-101-$SO_3H_{HCl}$ still shows some distinct diffraction peaks, the diffraction peaks of the recovered catalysts are not as obvious as the diffraction peaks of the fresh catalyst, in accordance with the performance of the $N_2$ isotherms.

## 4. Conclusions

A comparison of MIL-101-$SO_3H$ prepared by a one-pot synthesis using three different mineralizers to catalyze the esterification of cyclohexene with formic acid, highlighted the relatively better catalytic effect and stability of MIL-101-$SO_3H$ prepared by HCl as a mineralizer. The catalytic action was retained up to three run times. However, the catalyst structure underwent significant changes as determined by XRD and $N_2$ adsorption characterization, because of the strong polarity of the reaction solution and the limited tolerance of the catalyst. Further work should be conducted to improve the acid amount of MIL-101-$SO_3H$ and remain it better stability in a strongly polar system.

## Conflicts of interest

There are no conflicts to declare.

## Acknowledgements

This study was supported financially by the National Natural Science Foundation of China (No. 21776237) and Hunan 2011 Collaborative Innovation Center of New Chemical Technologies for Environmental Benignity and Efficient Resource Utilization.

## References

1 J. Long, S. Shu, Q. Wu, *et al.*, Selective cyclohexanol production from the renewable lignin derived phenolic chemicals catalyzed by Ni/MgO, *Energy Convers. Manage.*, 2015, **105**, 570–577.
2 E. L. Pires, J. C. Magalhães and U. Schuchardt, Effects of oxidant and solvent on the liquid-phase cyclohexane oxidation catalyzed by Ce-exchanged zeolite Y, *Appl. Catal., A*, 2000, **203**(2), 231–237.
3 Y. Hong, D. Sun and Y. Fang, The highly selective oxidation of cyclohexane to cyclohexanone and cyclohexanol over VAlPO4 berlinite by oxygen under atmospheric pressure, *Chem. Cent. J.*, 2018, **12**(1), 1–9.
4 T. Qiu, C. Kuang, C. Li, *et al.*, Study on Feasibility of Reactive Distillation Process for the Direct Hydration of Cyclohexene to Cyclohexanol Using a Cosolvent, *Ind. Eng. Chem. Res.*, 2013, **52**(24), 8139–8148.
5 F. Steyer and K. Sundmacher, Cyclohexanol Production *via* Esterification of Cyclohexene with Formic Acid and Subsequent Hydration of the Ester Reaction Kinetics, *Ind. Eng. Chem. Res.*, 2007, **46**(4), 1099–1104.
6 F. Steyer, H. Freund and K. Sundmacher, A Novel Reactive Distillation Process for the Indirect Hydration of Cyclohexene to Cyclohexanol Using a Reactive Entrainer, *Ind. Eng. Chem. Res.*, 2008, **47**(23), 9581–9587.
7 R. Ahamed Imam, H. Freund, R. P. M. Guit, *et al.*, Evaluation of Different Process Concepts for the Indirect Hydration of Cyclohexene to Cyclohexanol, *Org. Process Res. Dev.*, 2013, **17**(3), 343–358.
8 R. Kumar, A. Katariya, H. Freund, *et al.*, Development of a Novel Catalytic Distillation Process for Cyclohexanol Production: Mini Plant Experiments and Complementary Process Simulations, *Org. Process Res. Dev.*, 2011, **15**(3), 527–539.
9 A. Chakrabarti and M. M. Sharma, Cyclohexanol from cyclohexene *via* cyclohexyl acetate: catalysis by ion-exchange resin and acid-treated clay, *React. Polym.*, 1992, **18**(2), 107–115.
10 W. Xue, H. P. Zhao, J. Yao, *et al.*, Esterification of cyclohexene with formic acid over a peanut shell - derived carbon solid acid catalyst, *Chin. J. Catal.*, 2016, **37**(5), 769–777.
11 F. Steyer and K. Sundmacher, VLE and LLE Data Set for the System Cyclohexane + Cyclohexene + Water + Cyclohexanol + Formic Acid + Formic Acid Cyclohexyl Ester, *J. Chem. Eng. Data*, 2005, **50**(4), 1277–1282.
12 D. Wenming, X. Wei, L. Fang and W. Yanji, Study on the catalytic synthesis of cyclohexanol from cyclohexene *via* cyclohexyl formate, *J. Hebei Univ. Technol.*, 2012, **41**(04), 34–39.
13 W. Liu and C. Tan, Liquid-Phase Esterification of Propionic Acid with n-Butanol, *Ind. Eng. Chem. Res.*, 2001, **40**(15), 3281–3286.

14 G. Akiyama, R. Matsuda, H. Sato, *et al.*, Cellulose Hydrolysis by a New Porous Coordination Polymer Decorated with Sulfonic Acid Functional Groups, *Adv. Mater.*, 2011, **23**(29), 3294–3297.

15 Y. Zhou, Y. Chen, Y. Hu, *et al.*, MIL-101-$SO_3$H: A Highly Efficient Brønsted Acid Catalyst for Heterogeneous Alcoholysis of Epoxides under Ambient Conditions, *Chem.–Eur. J.*, 2014, **20**(46), 14976–14980.

16 Y. Jin, J. Shi, F. Zhang, *et al.*, Synthesis of sulfonic acid-functionalized MIL-101 for acetalization of aldehydes with diols, *J. Mol. Catal. A: Chem.*, 2014, **383–384**, 167–171.

17 L. Xiao-Fang, H. Li, H. Zhang, *et al.*, Efficient conversion of furfuryl alcohol to ethyl levulinate with sulfonic acid-functionalized MIL-101(Cr), *Chin. J. Catal.*, 2016, **6**, 90232–90238.

18 Y. Zang, J. Shi, F. Zhang, *et al.*, Sulfonic acid-functionalized MIL-101 as a highly recyclable catalyst for esterification, *Catal. Sci. Technol.*, 2013, **3**(8), 2044–2049.

19 B. Lu, Z. Wu, L. Ma, *et al.*, Phosphotungstic acid immobilized on sulphonic-acid-functionalized SBA-15 as a stable catalyst for the esterification of cyclohexene with formic acid, *J. Taiwan Inst. Chem. Eng.*, 2018, **88**, 1–7.

20 Q. Yang, M. P. Kapoor and S. Inagaki, Sulfuric Acid-Functionalized Mesoporous Benzene−Silica with a Molecular-Scale Periodicity in the Walls, *J. Am. Chem. Soc.*, 2002, **124**(33), 9694–9695.

21 P. Kim, Y. You, H. Park, *et al.*, Separation of $SF_6$ from $SF_6/N_2$ mixture using metal–organic framework MIL-100(Fe) granule, *Chem. Eng. J.*, 2015, **262**, 683–690.

22 A. Dhakshinamoorthy, M. Opanasenko, J. Í. Ejka, *et al.*, Metal organic frameworks as heterogeneous catalysts for the production of fine chemicals, *Catal. Sci. Technol.*, 2013, **3**(1), 254–259.

23 G. Férey, C. Mellot-Draznieks, C. Serre, *et al.*, A Chromium Terephthalate-Based Solid with Unusually Large Pore Volumes and Surface Area, *Science*, 2005, **5743**(309), 2040–2042.

24 Y. Lee, J. Kim and W. Ahn, Synthesis of metal-organic frameworks: a mini review, *Korean J. Chem. Eng.*, 2013, **30**(9), 1667–1680.

25 S. Bernt, V. Guillerm, C. Serre, *et al.*, Direct covalent post-synthetic chemical modification of Cr-MIL-101 using nitrating acid, *Chem. Commun.*, 2011, **47**(10), 2838–2840.

26 Z. Huang and H. K. Lee, Performance of metal-organic framework MIL-101 after surfactant modification in the extraction of endocrine disrupting chemicals from environmental water samples, *Talanta*, 2015, **143**, 366–373.

27 J. Juan-Alca Iz, R. Gielisse, A. B. Lago, *et al.*, Towards acid MOFs – catalytic performance of sulfonic acid functionalized architectures, *Catal. Sci. Technol.*, 2013, **3**(9), 2311–2318.

28 D. Li, D. Mao, J. Li, *et al.*, *In situ*-functionalized sulfonic copolymer toward recyclable heterogeneous catalyst for efficient Beckmann rearrangement of cyclohexanone oxime, *Appl. Catal., A*, 2016, **510**, 125–133.

29 D. Hong, Y. K. Hwang, C. Serre, *et al.*, Porous Chromium Terephthalate MIL-101 with Coordinatively Unsaturated Sites: Surface Functionalization, Encapsulation, Sorption and Catalysis, *Adv. Funct. Mater.*, 2009, **19**(10), 1537–1552.

30 M. G. Goesten, J. Juan-Alcañiz, E. V. Ramos-Fernandez, *et al.*, Sulfation of metal–organic frameworks: opportunities for acid catalysis and proton conductivity, *J. Catal.*, 2011, **281**(1), 177–187.

31 Z. Li, G. He, Y. Zhao, *et al.*, Enhanced proton conductivity of proton exchange membranes by incorporating sulfonated metal-organic frameworks, *J. Power Sources*, 2014, **262**, 372–379.

32 Z. Hasan, J. W. Jun and S. H. Jhung, Sulfonic acid-functionalized MIL-101(Cr): an efficient catalyst for esterification of oleic acid and vapor-phase dehydration of butanol, *Chem. Eng. J.*, 2015, **278**, 265–271.

33 A. J. Crisci, M. H. Tucker, M. Lee, *et al.*, Acid-Functionalized SBA-15-Type Silica Catalysts for Carbohydrate Dehydration, *ACS Catal.*, 2011, **1**(7), 719–728.

34 K. Hossein, H. A. Stil, H. P. C. E. Kuipers, *et al.*, Shape and Transition State Selective Hydrogenations using Egg-Shell Pt-MIL-101(Cr) Catalyst, *ACS Catal.*, 2013, **11**(3), 2617–2626.

35 Y. F. Chen, R. Babarao, S. I. Sandler, *et al.*, Metal−Organic Framework MIL-101 for Adsorption and Effect of Terminal Water Molecules: From Quantum Mechanics to Molecular Simulation, *Langmuir*, 2010, **26**(11), 8743–8750.

36 X. Du, X. Li, H. Tang, *et al.*, A Facile 2H-Chromene Dimerization Through an Ortho-Quinone Methide Intermediate Catalyzed by a Sulfonyl Derived MIL-101 MOF, *New J. Chem.*, 2018, **42**(15), 12722–12728.